

See discussions, stats, and author profiles for this publication at: <https://www.researchgate.net/publication/281303951>

Direct Measurement of the Nanomechanical Stability of a Redox Protein Active Site and Its Dependence upon Metal Binding

ARTICLE *in* THE JOURNAL OF PHYSICAL CHEMISTRY B · AUGUST 2015

Impact Factor: 3.3 · DOI: 10.1021/acs.jpcc.5b06382

READS

66

6 AUTHORS, INCLUDING:



Marina I Giannotti

University of Barcelona

30 PUBLICATIONS 359 CITATIONS

SEE PROFILE



Juan Manuel Artés

VU University Amsterdam

18 PUBLICATIONS 162 CITATIONS

SEE PROFILE



Fausto Sanz

University of Barcelona

190 PUBLICATIONS 2,953 CITATIONS

SEE PROFILE



Pau Gorostiza

IBEC Institute for Bioengineering of Catalonia

112 PUBLICATIONS 2,710 CITATIONS

SEE PROFILE

1 Direct Measurement of the Nanomechanical Stability of a Redox 2 Protein Active Site and Its Dependence upon Metal Binding

3 Marina I. Giannotti,^{*,†,‡,§} Israel Cabeza de Vaca,^{||} Juan M. Artés,^{‡,§,#} Fausto Sanz,^{†,‡,§} Victor Guallar,^{||,⊥}
4 and Pau Gorostiza^{*,†,§,⊥}

5 [†]Networking Biomedical Research Center on Bioengineering, Biomaterials and Nanomedicine (CIBER-BBN), Madrid 28029, Spain

6 [‡]Physical Chemistry Department, Universitat de Barcelona, Barcelona 08028, Spain

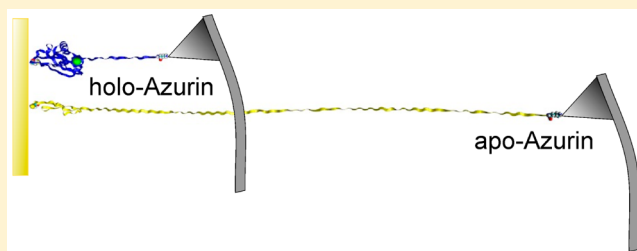
7 [§]Institute for Bioengineering of Catalonia (IBEC), Baldiri Reixac 15-21, Barcelona 08028, Spain

8 ^{||}Joint BSC-CRG-IRB Research Program in Computational Biology, Barcelona Supercomputing Center, Jordi Girona 29, Barcelona
9 08034, Spain

10 [⊥]Catalan Institution for Research and Advanced Studies (ICREA), Barcelona 08010, Spain

11 Supporting Information

12 **ABSTRACT:** The structural basis of the low reorganization
13 energy of cupredoxins has long been debated. These proteins
14 reconcile a conformationally heterogeneous and exposed
15 metal-chelating site with the highly rigid copper center
16 required for efficient electron transfer. Here we combine
17 single-molecule mechanical unfolding experiments with stat-
18 istical analysis and computer simulations to show that the
19 metal-binding region of apo-azurin is mechanically flexible and
20 that high mechanical stability is imparted by copper binding.
21 The unfolding pathway of the metal site depends on the
22 pulling residue and suggests that partial unfolding of the metal-binding site could be facilitated by the physical interaction with
23 certain regions of the redox protein.



24 INTRODUCTION

25 Protein-mediated electron transfer (ET) reactions are essential
26 in many biological processes, such as cellular respiration and
27 photosynthesis.^{1,2} At the low electrochemical driving forces
28 found in most biological systems, the extraordinary efficiency of
29 such processes is based on the maximization of the coupling
30 between donor and acceptor and the optimization of the
31 reorganization energy.^{2–4} Many redox proteins host in their
32 structures transition metal ions like copper and iron, whose
33 electrochemical properties can be tuned by the protein
34 environment to meet the requirements of the biological ET.⁵
35 In iron centers, rigid cofactors like the heme group are used to
36 avoid high reorganization energies when cycling between the
37 geometries preferred by the metal in the different redox states.⁵
38 In contrast, copper ions are bound directly to flexible protein
39 residues, and the rigidity relies upon the protein folding. The
40 entatic/rack-induced state model^{6,7} suggests that a metal-
41 chelating site is preformed in the protein to impart rigidity
42 regardless of the presence of the ion, in agreement with the
43 virtually identical structure of holo- and apo-cupredoxins^{8,9} and
44 the minimized conformational changes during Cu^{II}/Cu^I redox
45 cycling.^{10,11}

46 These views were challenged by the discovery of copper
47 metallochaperones,¹² which load the metal ion into cupredox-
48 ins following a mechanism that requires an exposed metal-
49 binding site and protein–protein interactions¹³ that are

incompatible with a hidden, rigid metal site. In addition, so
structural evidence of conformational heterogeneity of the
metal-binding site in cupredoxins^{14–17} suggests that the metal
binding may contribute to their rigidity and that flexibility in
the chelating site may be essential for metallochaperone-
mediated copper binding *in vivo*. However, no direct evidence
on the mechanical stability of the protein¹⁸ and its relation to
the coordination site has yet been reported. The mechanical
lability¹⁹ of metal–protein bonds has major relevance for the
structure and function of redox metalloproteins, but it is
difficult to characterize using classical structural techniques and
thermal or chemical denaturation methods. In order to directly
measure the mechanical properties of the Cu-binding region of
a cupredoxin and to assess the effect of the metal, we have
mechanically unfolded individual azurin (Az) molecules using
single-molecule force spectroscopy (SMFS) with an atomic
force microscope (AFM).^{18,20–25} In particular, we compared
the holo and apo forms of Az (with and without the Cu ion,
respectively) using force–extension curves, statistical analysis,
and computational simulations. Protein unfolding experiments
mediated by mechanical force (SMFS) constitute kinetic rather
than thermodynamic measurements, and therefore mechanical

Received: July 3, 2015

Revised: August 14, 2015



unfolding pathways may differ from chemical unfolding ones.^{26,27} However, SMFS provides useful insights on protein structure–activity relationships and on the physiological interaction between protein partners that complement those results obtained by *in vitro* denaturation experiments using nonphysiological temperatures or chemical agents like urea.

RESULTS AND DISCUSSION

Mechanical Unfolding of Individual Holo and Apo-Az: Single-Molecule Force Spectroscopy.

Holo- and apo-Az display nearly identical tertiary structure^{8,9} and thus provide an opportunity to directly determine the role of the metal in Az mechanical stability using AFM-SMFS. We chose wild-type monomeric Az for several reasons, despite the difficulty of the recordings and data analysis compared to multidomain proteins often used in SMFS. Monomers are more biologically relevant and enable a direct comparison with bulk experiments performed with cupredoxins. In addition, using wild-type monomeric Az allows avoiding structural alterations introduced by molecular handles, domain–domain interactions, and aggregation problems of multidomain proteins. In order to orient the Cu site of Az toward the AFM probe, we chemisorbed the protein on an atomically flat gold surface via native cysteine residues (Cys3 and Cys26),^{28–30} and we performed force spectroscopy experiments in buffer solution.

To perform SMFS experiments, the tip of a flexible AFM cantilever was approached to the surface and attached nonspecifically to the protein. Unfolding force–extension profiles were recorded upon tip retraction, until the tip–protein contact was ruptured at force F_r and length l_r , both for holo- and apo-Az (Figure 1). Because the interaction between the protein and the AFM tip is nonspecific, the tip can make contact and “grab” the protein from different solvent-exposed residues along the chain, and thus different portions of the protein can be stretched and unfolded. The force–extension traces were normalized by the extension corresponding to 110 and 150 pN for holo-Az and for apo-Az data sets, respectively. Different normalized force curves for each data set can be superimposed, confirming that single molecules are being stretched^{31,32} (Figure S1). The contact between the probe and holo-Az is ruptured at l_r around 8 nm, while values of l_r are distributed more broadly for apo-Az (5–30 nm, Figure 2a). The distribution of rupture forces F_r is similar in both cases, indicating that the tip–protein interactions are comparable. As the tertiary structures of holo-Az and apo-Az are nearly identical, the differences in l_r recorded values may only indicate that the presence of the copper ion changes the mechanical properties of individual Az proteins. Apo-Az is easier to stretch and unfold, and the variation in l_r reflects that the protein is picked up and extended from different residues. In contrast, the maximum extension of holo-Az stays around 8 nm for forces up to 300–400 pN, regardless of the pulling residue. As a control we used denatured Az (den-Az) and representative force–extension plots are displayed in Figure 3a. The probability of stretching den-Az from diverse residues along the chain is independent of F_r , with l_r values ranging from 4 to 40 nm (Figure 3b), in agreement with the total length of the protein.

The forced extension of the unfolding polypeptide chain can generally be described using the worm-like chain (WLC) model for polymer stretching.³³ Force–extension curves were fitted to the WLC model (black lines in Figure 1a) to obtain the persistence length l_p and contour length L_c .³⁴ The WLC model represents a simplified situation in which the force opposed to

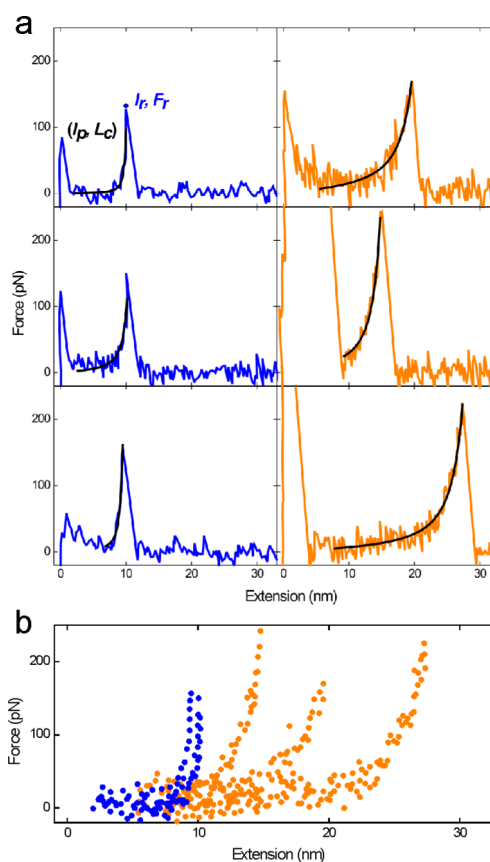


Figure 1. AFM-SMFS force–extension curves. (a) Representative AFM-SMFS force–extension traces of individual holo-Az (blue curves) and apo-Az (orange curves) in 50 mM ammonium acetate buffer pH 4.5, at 25 °C. Black continuous lines correspond to the fitting of the experimental data to the worm-like chain (WLC) model. (b) Superposition of the pulling traces shown in part a.

the elongation of the macromolecule is mainly driven by entropy. However, the apparent persistence length resulting from WLC fits to protein unfolding data from AFM experiments generally reflects a phenomenological stiffness, comprising effects due to both chain entropy and hydrophobic collapse. Typically, l_p values around 0.4 nm are found when the WLC model is used to describe the elastic behavior of proteins.^{35–38} For apo-Az, plots of l_p versus L_c shown in Figure 2b yield an average l_p value of 0.5 ± 0.3 nm, similar to other polypeptides. In addition, l_p is independent of the maximum force attained during unfolding (Figure 4), which indicates that for apo-Az the mechanical properties obtained from the WLC fit are consistent at all extension values. In contrast, holo-Az curves are not well-fit by the WLC model: l_p displays a wider distribution (0.8 ± 1.2 nm), and a dependence with the rupture force (the highest l_p values were obtained when rupture occurred at low F_r , see Figure 4). In part, this is related to the average stretching length being too small to be described by WLC. In addition, these deviations are usually associated with the presence of strong intramolecular interactions that are “softened” upon extension.³⁹ In holo-Az, these intraprotein interactions must be due to the presence of the metal. Indeed, disruption of these interactions could be the cause of the change in the macromolecular elasticity properties while extension increases, giving rise to broad distribution of l_p values and a dependence on the maximum force attained (F_r). As expected from the l_r values observed, contour lengths

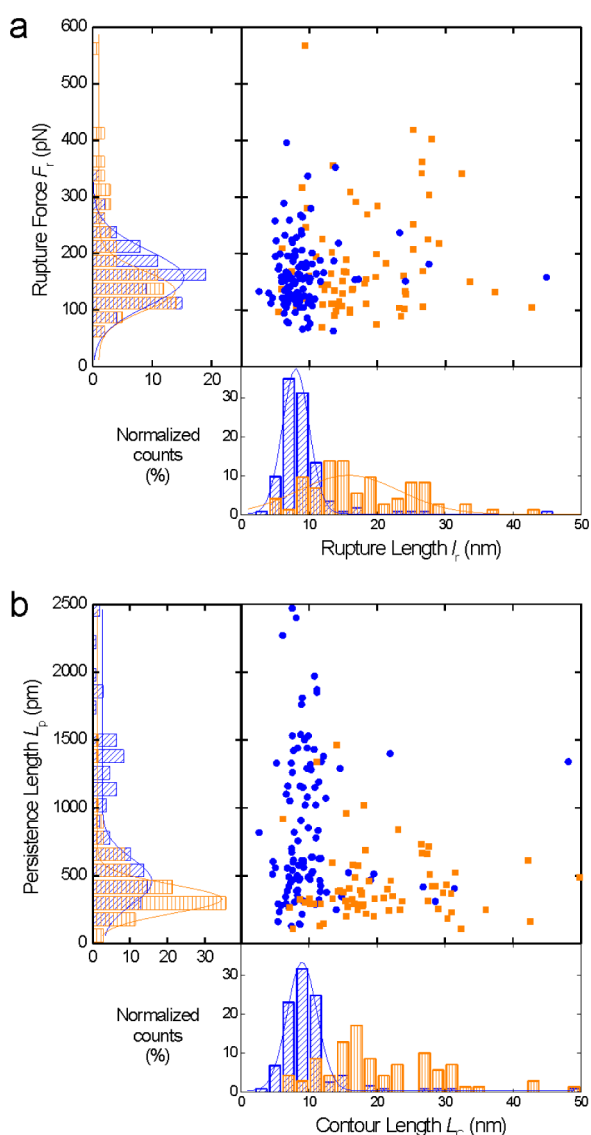


Figure 2. AFM-SMFS and WLC model. Distribution of (a) rupture force (F_r) and length (l_r); (b) persistence (l_p) and contour length (L_c) parameters obtained from fitting the experimental data to the WLC model, for AFM-SMFS of individual holo-Az (blue) and apo-Az (orange) in 50 mM ammonium acetate buffer pH 4.5, at 25 °C.

L_c are centered on 9 nm for holo-Az and broadly distributed for apo-Az (8–35 nm). Compared to apo- and holo-Az curves, the elastic behavior of den-Az control curves (Figure 3a) was described well by the WLC model, with a value for the average persistence length of $l_p = 0.3 \pm 0.1$ nm, and contour length L_c up to 45 nm, in accordance with the l_r values obtained experimentally.

In brief, SMFS experiments reveal that apo-Az can be mechanically extended to the total length of the unfolded protein, while holo-Az can be extended to a maximum of approximately 8 nm. Clear deviations of the force–extension from the WLC model for holo-Az indicate the presence of strong intraprotein interactions when the metal is bound. Since the X-ray structures of holo-Az and apo-Az are almost identical, these results demonstrate that the presence of the copper ion increases the mechanical stability of the protein structure at the metal-binding site, and prevents the complete unfolding of

holo-Az in SMFS experiments based on nonspecific tip–protein interactions (maximum force attained 300–400 pN).

Molecular View of the Force–Extension Differences between Apo- and Holo-Az: Computational Simulations.

The variability observed in SMFS experiments of Az could not be reduced by increasing the number of experiments, probably due to the concurrence of intrinsically variable conditions like the structural configuration of the protein and the different attachment residues to the AFM tip. In order to gain insight into these variables, we turned to molecular simulations by using the protein energy landscape exploration (PELE, <https://pele.bsc.es>) software, and calculating the Az unfolding curves from most surface residues (Figure 5). This is the first time that PELE is used to simulate force–extension experiments on protein unfolding. Nevertheless, molecular dynamics have been largely used to simulate AFM-SMFS experiments to obtain an atomic description of force–extension profiles^{40–42} (see description of PELE and its comparison to molecular dynamics in Methods section). Due to computer limitations (classical force fields, pulling speed, etc.),⁴³ however, simulations result in force overestimation,^{42,44} and AFM modeling is based mostly in qualitative explorations.⁴³

In Figure 6 we present example profiles obtained for surface residue Lys128 in holo- and apo-Az simulations. These show that forces in the holo model are higher than in the apo model for a large fraction of the trajectory. The difference in extension at a constant force is shown in the snapshot (structure of partially unfolded protein) of Figure 6a and is calculated in Figure 7 for the entire range of force. As observed in the holo and apo-Az structure in Figure 6a, while apo-Az is almost fully extended, only part of the holo-Az is unfolded, between the coordination center and the pulling residue (Lys128) for this case. Figure 7a shows the holo and apo-Az difference in extension length between fixed (Cys26) and pulled (γ carbon of Lys128) atoms for every given force. This difference is highest at 3000 pN, as a result of a shorter extension in holo-Az due to the Cu interaction with its coordinating residues. Figure 7 also includes two snapshots of the atomic representation showing the metal coordination distances before pulling and after the peak for the pulling residue Lys128, and the final snapshot for residues Ala65 (Figure 7b) and Pro75 (Figure 7c) which display a markedly different behavior.

The expanded view of Figure 6b shows that, during holo-Az unfolding, the force increases abruptly at an extension of ca. 9 nm, whereas apo-Az unfolds at a relatively constant force in this range. This process can be observed in detail in the Supporting Information video S1, and indicates that the strength of the metal–residue interaction stabilizes the difference in extension for a significant force range (or extension time as seen in the video). Simulations were repeated for all residues shown in Figure 5, and the results are summarized in a force versus length plot (Figure 8) that reproduces the experimental observations of Figure 2a.

Compared to experimental curves, which sample several attachment residues on the protein surface and must be analyzed statistically (Figure 2a), in simulations specific residues can be selected to unfold the protein, and unfolding events can be individually tracked. Although calculated force values differ from experimental ones, simulations are not limited by the tip–protein force. Remarkably, both methods fully unfold apo-Az up to 40 nm, whereas holo-Az unfolding is restricted to (or the simulated force increases steeply at) lengths below 10 nm. The shorter extension in holo-Az is due

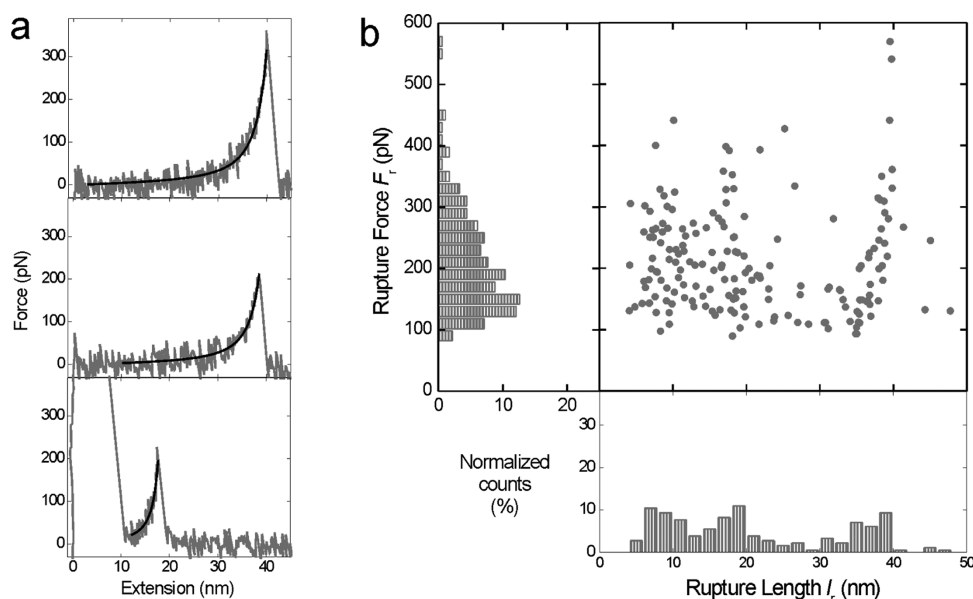


Figure 3. AFM-SMFS on den-Az. (a) Representative AFM-SMFS force–extension traces of individual den-Az in 4 M GuHCl and 50 mM ammonium acetate buffer pH 4.5, at 25 °C. Black continuous lines correspond to the fitting of the experimental data to the worm-like chain (WLC) model. (b) Distribution of rupture forces (F_r) and lengths (l_r) for individual den-Az.

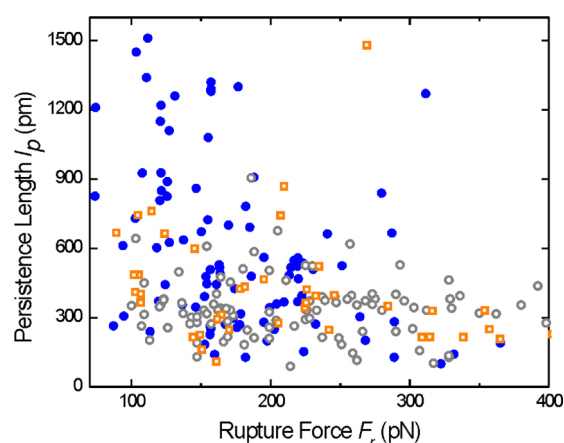


Figure 4. WLC: variation of l_p with F_r . Persistence length (l_p), obtained from fitting the experimental data to the WLC model, vs rupture force (F_r), for individual holo-Az (blue), apo-Az (orange) (in 50 mM ammonium acetate buffer pH 4.5), and den-Az (gray) (in 4 M GuHCl and 50 mM ammonium acetate buffer pH 4.5, at 25 °C).

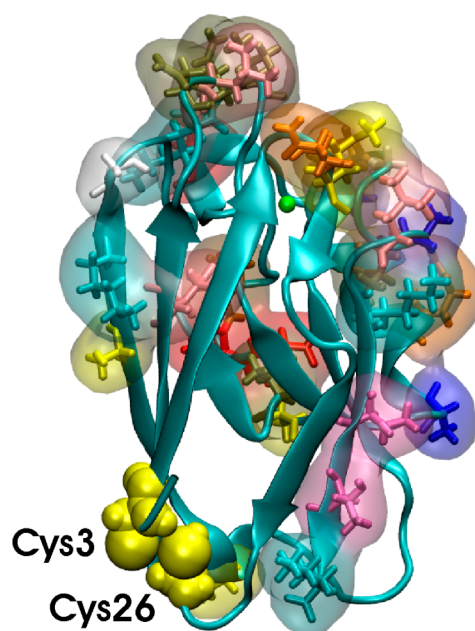


Figure 5. Three-dimensional structure of *Pseudomonas aeruginosa* Az where all residues analyzed are highlighted. The substrate-attaching residues Cys3 and Cys26 (yellow balls) were fixed in the simulations. The copper ion is represented by a green sphere in the region facing the AFM probe. Color code for the highlighted residues: Met (yellow), Asp (red), Ala (blue), Asn (dark green), Lys (cyan), Glu (pink), Gln (orange), Gly (white).

241 to the Cu interaction with its coordination residues. For every
 242 simulated attachment site, the divergence between the apo- and
 243 holo-Az extension is accompanied by strain and eventual
 244 rupture of metal coordination bonds in the holo-case (Figure
 245 6b, Figure 7, and video S1), following different unfolding
 246 sequences (as exemplified in Figure 7 for pulling residues
 247 Lys128, Pro75, and Ala65). Together, these results indicate that
 248 the metal-binding region is mechanically flexible when the
 249 metal is not coordinated, and Cu coordination prevents the full
 250 extension of the protein regardless of the attachment site. Our
 251 results are in accordance with reported observations of
 252 conformational heterogeneities for the metal-binding site in
 253 cupredoxins in absence of the metal and their suggestion of
 254 the contribution of the metal ion to the rigidity.^{14–16,45}
 255 Interestingly, the dependence of the unfolding sequence on
 256 the pulling residue selected in the simulations suggests that
 257 partial unfolding of the metal-binding site could be facilitated

by the physical interaction with certain regions of the redox 258
 protein. In other words, residues providing active site unfolding 259
 at low forces might belong to a functional region of the redox 260
 protein involved in metal loading, a sort of “pull tab” that could 261
 be mechanically stretched by copper chaperones through 262
 specific protein–protein interactions. Indeed, several copper- 263
 mediated protein–protein interactions have been identified in 264
 recent years,^{46,47} and in some cases the crystal structures 265
 involve the copper ion along with direct interactions between 266

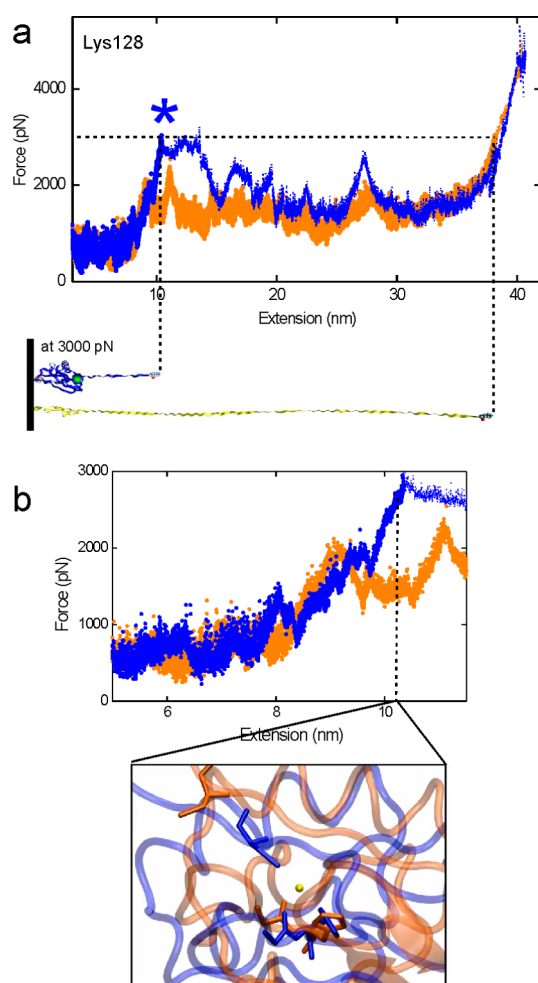


Figure 6. PELE force–extension. (a) PELE force–extension profile for surface residue Lys128 of holo-Az (blue) and apo-Az (orange). The asterisk (*) indicates the maximum extension value obtained experimentally for holo-Az. Apo and holo-Az unfolding at the force corresponding to * is also displayed. (b) Initial stage of unfolding and Cu-binding site conformation snapshots for holo-Az and apo-Az at 10 nm extension for Lys 128.

large protein surfaces.¹³ Furthermore, a deformation of the metal-binding site upon metallochaperone binding was observed by NMR⁴⁸ and is in agreement with MD simulations showing great flexibility in apoAz and especially in the binuclear CuA domain of cytochrome c oxidase.⁴⁵

CONCLUDING REMARKS

In summary, the copper binding site needed for efficient ET in azurin is mechanically flexible in apo-Az, and metal binding increases its mechanical stability. The mechanical stability of metal-binding proteins and its relevance to the structure and function of redox metalloproteins is difficult to characterize using classical structural techniques. Our findings suggest that the mechanism of copper loading into cupredoxins may implicate a mechanical contribution, in addition to the well-characterized chemical binding affinity of the metal.^{5,49–51}

METHODS

Sample Preparation. Native *Pseudomonas aeruginosa* azurin (holo-Az) and all reagents were purchased from Sigma. Apo-Az was obtained by removing the Cu ion from

the protein structure by titrating holo-Az with a solution 0.1 M KCN, as described.⁵² Denatured Az (den-Az) was obtained by keeping holo-Az in 4 M guanidine hydrochloride (GuHCl) solution in acetate buffer (pH 4.5). The apo-Az structure conservation and protein denaturation by GuHCl were followed by monitoring fluorescence from tryptophan Trp48, selectively excited at 290 nm (Figure S2), as the fluorescence maximum of native Az lies at ca. 310 nm and shifts to 350 nm when the protein unfolds.⁵³ Reported protocols were used to prepare atomically flat gold surfaces⁵⁴ and to attach Az on gold^{29,55} through native cysteines Cys3 and Cys26, which results in a defined orientation of the protein on the surface, while preserving its native-like conformation.^{56,57} In order to obtain isolated Az molecules on the gold surface, a solution of Az (holo, apo, or den) of ca. 5 $\mu\text{g mL}^{-1}$ in 50 mM ammonium acetate buffer (pH 4.5) was incubated for 2 h over the substrate and, afterward, extensively rinsed with buffer solution. All glassware used was cleaned with piranha solution (7:3 $\text{H}_2\text{SO}_4\text{:H}_2\text{O}_2$ (30%)). *Caution: Piranha solution should be handled with extreme caution.* Deionized water (18 $\text{M}\Omega\text{ cm}^{-1}$ Milli-Q, Millipore) was used to prepare all solutions and for substrate rinsing.

AFM-Based Single-Molecule Force Spectroscopy (SMFS) Measurements. SMFS was performed with an MFP-3D AFM (Asylum Research, Santa Barbara, CA). Force curves were acquired using V-shaped Si_3N_4 cantilevers (DNP, Bruker, AFM Probes, Camarillo, CA) with a nominal spring constant of 0.1 N m^{-1} . Individual spring constants were calibrated using the equipartition theorem (thermal noise routine).⁵⁸ All the measurements were performed at room temperature in 50 mM ammonium acetate buffer solution, pH = 4.5, previously filtered with 0.02 μm pore filters (Anotop 25 Plus, Whatman) for holo and apo-Az, and in 4 M GuHCl, 50 mM ammonium acetate solution, pH = 4.5, for den-Az. All the experiments were performed in the constant-velocity mode at 1 $\mu\text{m s}^{-1}$ approach and retract velocity. The total number of experimental stretch curves used in Figures 2 and 3 were 120 (holo-Az), 70 (apo-Az), and 182 (den-Az), from at least three different samples.

The experimental results were fitted to a model for single-chain elasticity of random coiled macromolecules, the worm-like chain (WLC) model.³⁴ The model describes a macromolecular chain as a homogeneous string with a constant bending elasticity and predicts the relationship between extension and entropic restoring force generated for a polymer chain. WLC has been effectively used to reproduce the force–extension behavior, at short extensions, of certain synthetic macromolecules³² and many biomacromolecules, such as DNA³³ and proteins.^{59,60} Both l_p and L_c were used as fitting parameters. The force (F) versus extension (x) interpolation formula of Marko and Siggia⁶¹ was used:

$$F(x) = \frac{k_b T}{l_p} \left[\frac{1}{4} \left(1 - \frac{x}{L_c} \right)^{-2} + \frac{x}{L_c} - \frac{1}{4} \right] \quad (1)$$

PELE Computational Simulations. PELE is a Monte Carlo method originally developed for exploring the configurational space of protein–ligand recognition. Each Monte Carlo step is composed of three main moves: localized perturbation, side chain sampling, and global minimization. The localized perturbation is based on applying anisotropic normal modes (ANM) to the protein in order to describe conformational changes. Additionally, if a ligand is present, it might include its

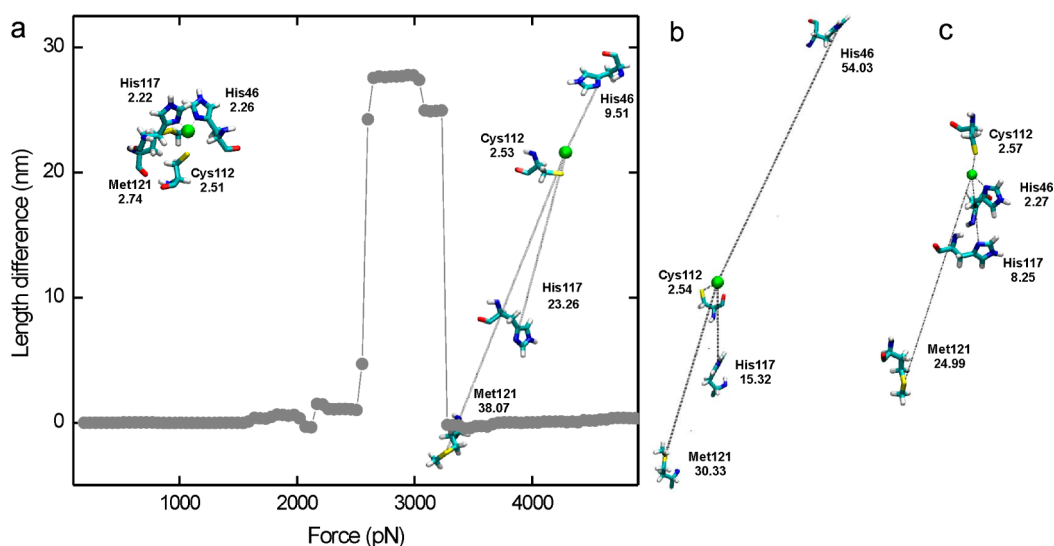


Figure 7. PELE molecular view of the force–extension: (a) Difference in extension (length difference) between the holo and apo-Az obtained by PELE at every given force for residue Lys128. Schematics of the distance between the Cu atom and four of its coordination residues (His46, Cys112, His117, and Met121) before and after the maximum force peak at 3000 pN for pulling residues Lys128 (a), Ala65 (b), and Pro75 (c).

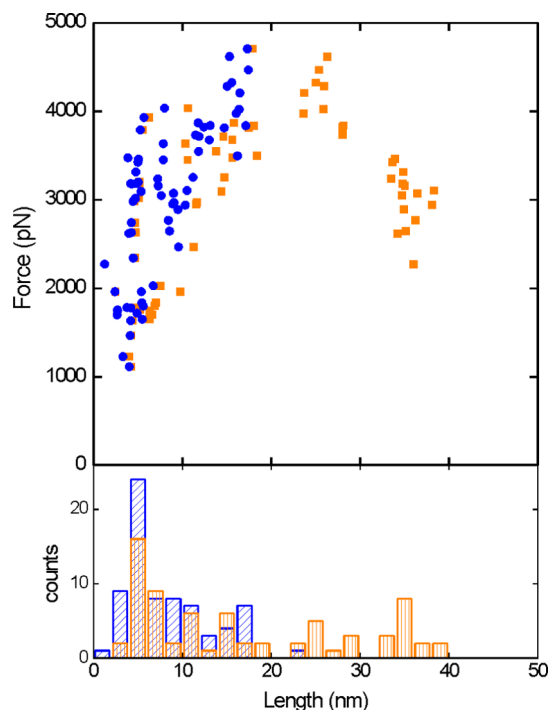


Figure 8. Force vs length obtained from all PELE simulations (see Data Analysis section) for holo (blue) and apo-Az (orange).

step the VP is displaced by a fixed amount in a desired 358 direction. The VP starting position is the same as the restrained 359 atom, giving an initial force of zero. Then, each PELE iteration 360 computes the harmonic force induced by the VP motion, 361 modeling the corresponding force measured by the cantilever. 362 In this study, the lowest 15 ANM modes were chosen, and 363 updated every 10 steps. The force constants used in the 364 harmonic VP constraint were set to 10 kcal/mol Å². Cys3 and 365 Cys26 were fixed with a large harmonic constraint, modeling its 366 surface attachment. 367

SMD has been largely used to simulate AFM-SMFS 368 experiments in order to obtain an atomic description of 369 unfolding force–extension profiles.^{40–42} Monte Carlo methods 370 (such as PELE) are traditionally seen as an alternative to 371 molecular dynamics (MD) techniques. Using PELE, for 372 example, we have recently shown the capability of reproducing 373 protein dynamics at a considerably faster rate than MD.⁶² 374 These technological advances open the possibilities of 375 modeling multiple experiments in a timely manner involving, 376 for example, different initial conditions or pulling residues. In 377 order to validate our new approach with an established 378 technique, such as SMD, we also performed SMD simulations 379 for Lys128. See Supporting Information for SMD simulation 380 setup details. As seen in Figure S3, SMD provides the same 381 results as PELE but at the expense of approximately 5 times 382 higher CPU cost. 383

System Setup. The crystal structure 4AZU⁸ was selected 384 from the protein data bank for the computational simulations. 385 The system was prepared with the Protein Preparation Wizard 386 tool,⁶³ adding missing hydrogen atoms, fixing environment 387 dependent protonation states, and checking disulfide bonds. 388 PELE uses the OPLSAA⁶⁴ force field with an implicit surface 389 generalized solvent model. The charge of the Cu ion was set to 390 +2. The ionic strength has been set to 0.15 mol dm^{−3}. Due to 391 the qualitative nature of our simulations, the metal coordination 392 bonds were described only by means of the force field 393 electrostatic term. To validate this approach, we performed 394 preliminary tests using a model with the Cu center plus the 5 395 coordinated ligands, where we built gas phase pulling energy 396 profiles in each coordination bond with both QM(M06/ 397

346 translation and rotation. The second move, side chain sampling, 347 uses rotamer libraries to explore different side chain 348 configurations as a response to the initial local perturbation. 349 Finally, the global minimization optimizes the energy of the 350 newly found configuration. More on PELE can be found in 351 several publications and online, <https://pele.bsc.es>, where the 352 software is freely available.

353 We have expanded the code to study single-molecule force 354 spectroscopy experiments such as AFM or optical tweezers, in a 355 similar fashion to steered molecular dynamics (SMD).⁴⁰ To this 356 aim we have added the possibilities of including atom harmonic 357 constraints to a moving virtual point (VP). Thus, at each MC

lacvp**) and OPLS levels of theory. Results were actually surprisingly good, and in 4 of the ligands (the two His, the Met, and the Gly, see Supporting Information Figure S4), the energy profiles were in qualitative (and even semiquantitative) agreement with quantum calculations; only breaking the Cu–Cys bond (charge separation) resulted in significant off-results (4× larger OPLS dissociation energies). Moreover, these gas phase differences were further reduced when adding electrostatic screening derived from the “condensed” protein media.

From experimental SMFS it is not possible to determine which residue is attached to the cantilever. For this reason, each simulation was performed with a randomly selected residue (to be pulled) from a surface list. The surface residues included the following: Gln12, Met13, Leu33, Asn38, Leu39, Lys41, Asn42, Val43, Ala54, Gln57, Val60, Ala65, Asp69, Pro75, Asp76, Asp77, Ser78, Val80, Gly90, Lys92, Ser94, Ser100, Pro115, Gly116, Ala119, Leu120, Lys122, Thr124, Thr126, Lys128 (Figure 5). Additionally, the atom to be restrained was chosen randomly between the carbons of the side chain.

Data Analysis. Three independent trajectories were performed for each selected residue and state. Then, the average force with respect to the extension was linearly interpolated in order to obtain a continuum force plot. The force peak corresponding to the largest difference in extension between the holo and apo-Az simulations was then selected as an indication of the “rupture force” (Figure 7a). Thus, for each of the residues analyzed (Figure 5) there are three pairs of points in Figure 8 (each pair containing one apo and one holo point from each independent simulation). Notice that by using this “rupture force”, instead of a fixed rupture force, we obtain possibly an upper bound value for the differences between apo and holo.

ASSOCIATED CONTENT

Supporting Information

The Supporting Information is available free of charge on the ACS Publications website at DOI: 10.1021/acs.jpcb.5b06382.

Figures showing validation of single-molecule force spectroscopy experiments, characterization of denatured azurin, molecular view (computational simulations) of the force–extension, and metal coordination bond analysis (PDF)

Video showing unfolding forces (AVI)

AUTHOR INFORMATION

Corresponding Authors

*E-mail: migiannotti@ub.edu.

*E-mail: pau@icrea.cat.

Present Address

[#]Department of Electrical and Computer Engineering, University of California Davis, One Shields Avenue, Davis, California 95616, United States.

Author Contributions

The manuscript was written through contributions of all authors. All authors have given approval to the final version of the manuscript. M.I.G. and I.C.d.V. contributed equally.

Notes

The authors declare no competing financial interest.

ACKNOWLEDGMENTS

We are grateful to A. Donaire and I. Díez-Pérez for discussions, and to the Catalan government (grant 2014SGR-1251), the Spanish government (grant CTQ2013-43892R) and the European Research Council (PELE ERC-2009-Adg 25027) for financial support.

REFERENCES

- (1) Ramirez, B. E.; Malmstrom, B. G.; Winkler, J. R.; Gray, H. B. The Currents of Life: The Terminal Electron-transfer Complex of Respiration. *Proc. Natl. Acad. Sci. U. S. A.* **1995**, *92* (26), 11949–11951.
- (2) Marcus, R. A.; Sutin, N. Electron Transfers in Chemistry and Biology. *Biochim. Biophys. Acta, Rev. Bioenerg.* **1985**, *811* (3), 265–322.
- (3) Gray, H. B.; Winkler, J. R. Long-range Electron Transfer. *Proc. Natl. Acad. Sci. U. S. A.* **2005**, *102* (10), 3534–3539.
- (4) Wallrapp, F. H.; Voityuk, A. A.; Guallar, V. In-silico Assessment of Protein-Protein Electron Transfer. A Case Study: Cytochrome c Peroxidase - Cytochrome c. *PLoS Comput. Biol.* **2013**, *9* (3), e1002990.
- (5) Winkler, J. R.; Wittung-Stafshede, P.; Leckner, J.; Malmstrom, B. G.; Gray, H. B. Effects of Folding on Metalloprotein Active Sites. *Proc. Natl. Acad. Sci. U. S. A.* **1997**, *94* (9), 4246–4249.
- (6) Lancaster, K. M.; Farver, O.; Wherland, S.; Crane, E. J., III; Richards, J. H.; Pecht, I.; Gray, H. B. Electron Transfer Reactivity of Type Zero Pseudomonas Aeruginosa Azurin. *J. Am. Chem. Soc.* **2011**, *133* (13), 4865–4873.
- (7) Vallee, B. L.; Williams, R. J. Metalloenzymes: The Entatic Nature of their Active Sites. *Proc. Natl. Acad. Sci. U. S. A.* **1968**, *59* (2), 498–505.
- (8) Nar, H.; Messerschmidt, A.; Huber, R.; van de Kamp, M.; Canters, G. W. Crystal Structure Analysis of Oxidized Pseudomonas Aeruginosa Azurin at pH 5.5 and pH 9.0: A pH-Induced Conformational Transition Involves a Peptide Bond Flip. *J. Mol. Biol.* **1991**, *221* (3), 765–772.
- (9) Nar, H.; Messerschmidt, A.; Huber, R.; van de kamp, M.; Canters, G. W. Crystal-Structure Of Pseudomonas-Aeruginosa Apo-Azurin At 1.85 Angstrom Resolution. *FEBS Lett.* **1992**, *306* (2–3), 119–124.
- (10) Malmström, B. G. Rack-induced Bonding in Blue-Copper Proteins. *Eur. J. Biochem.* **1994**, *223* (3), 711–718.
- (11) Gray, H. B.; Malmström, B. G.; Williams, R. J. P. Copper Coordination in Blue Proteins. *JBIC, J. Biol. Inorg. Chem.* **2000**, *5* (5), 551–559.
- (12) Rae, T. D.; Schmidt, P. J.; Pufahl, R. A.; Culotta, V. C.; O'Halloran, T. V. Undetectable Intracellular Free Copper: The Requirement of a Copper Chaperone for Superoxide Dismutase. *Science* **1999**, *284* (5415), 805–808.
- (13) Banci, L.; Bertini, I.; Cantini, F.; Felli, I. C.; Gonnelli, L.; Hadjiladis, N.; Pierattelli, R.; Rosato, A.; Voulgaris, P. The Atx1-Ccc2 Complex is a Metal-Mediated Protein-Protein Interaction. *Nat. Chem. Biol.* **2006**, *2* (7), 367–368.
- (14) Ryde, U.; Olsson, M. H. M.; Roos, B. r. O.; De Kerpel, J. O. A.; Pierloot, K. On the Role of Strain in Blue Copper Proteins. *JBIC, J. Biol. Inorg. Chem.* **2000**, *5* (5), 565–574.
- (15) Messerschmidt, A.; Prade, L.; Kroes, S. J.; Sanders-Loehr, J.; Huber, R.; Canters, G. W. Rack-Induced Metal Binding vs. Flexibility: Met121His Azurin Crystal Structures at Different pH. *Proc. Natl. Acad. Sci. U. S. A.* **1998**, *95* (7), 3443–3448.
- (16) Zaballa, M. E.; Abriata, L. A.; Donaire, A.; Vila, A. J. Flexibility of the Metal-Binding Region in Apo-Cupredoxins. *Proc. Natl. Acad. Sci. U. S. A.* **2012**, *109* (24), 9254–9259.
- (17) Warren, J. J.; Lancaster, K. M.; Richards, J. H.; Gray, H. B. Inner- and Outer-Sphere Metal Coordination in Blue Copper Proteins. *J. Inorg. Biochem.* **2012**, *115*, 119–126.
- (18) Rico, F.; Rigato, A.; Picas, L.; Scheuring, S. Mechanics of Proteins with a Focus on Atomic Force Microscopy. *J. Nanobiotechnol.* **2013**, *11* (Suppl 1), S3.

- (19) Zheng, P.; Takayama, S.-i. J.; Mauk, A. G.; Li, H. Hydrogen Bond Strength Modulates the Mechanical Strength of Ferric-Thiolate Bonds in Rubredoxin. *J. Am. Chem. Soc.* **2012**, *134* (9), 4124–4131.
- (20) Shi, W.; Giannotti, M. I.; Zhang, X.; Hempenius, M. A.; Schönherr, H.; Vancso, G. J. Closed Mechanoelectrochemical Cycles of Individual Single-Chain Macromolecular Motors by AFM. *Angew. Chem., Int. Ed.* **2007**, *46* (44), 8400–8404.
- (21) Nash, M. A.; Gaub, H. E. Single-Molecule Adhesion of a Stimuli-Responsive Oligo(ethylene glycol) Copolymer to Gold. *ACS Nano* **2012**, *6* (12), 10735–10742.
- (22) Zheng, P.; Wang, Y.; Li, H. Reversible Unfolding–Refolding of Rubredoxin: A Single-Molecule Force Spectroscopy Study. *Angew. Chem., Int. Ed.* **2014**, *53* (51), 14060–14063.
- (23) Farrance, O. E.; Paci, E.; Radford, S. E.; Brockwell, D. J. Extraction of Accurate Biomolecular Parameters from Single-Molecule Force Spectroscopy Experiments. *ACS Nano* **2015**, *9* (2), 1315–1324.
- (24) Van Quaethem, A.; Lussis, P.; Leigh, D. A.; Duwez, A.-S.; Fustin, C.-A. Probing the Mobility of Catenane Rings in Single Molecules. *Chem. Sci.* **2014**, *5* (4), 1449–1452.
- (25) Giannotti, M. I.; Rinaudo, M.; Vancso, G. J. Force Spectroscopy of Hyaluronan by Atomic Force Microscopy: From Hydrogen-Bonded Networks toward Single-Chain Behavior. *Biomacromolecules* **2007**, *8* (9), 2648–2652.
- (26) Jagannathan, B.; Elms, P. J.; Bustamante, C.; Marqusee, S. Direct observation of a force-induced switch in the anisotropic mechanical unfolding pathway of a protein. *Proc. Natl. Acad. Sci. U. S. A.* **2012**, *109* (44), 17820–17825.
- (27) Wittung-Stafshede, P. Role of Cofactors in Protein Folding. *Acc. Chem. Res.* **2002**, *35* (4), 201–208.
- (28) Friis, E. P.; Andersen, J. E. T.; Madsen, L. L.; Bonander, N.; Moller, P.; Ulstrup, J. Dynamics of Pseudomonas Aeruginosa Azurin and its Cys3Ser Mutant at Single-Crystal Gold Surfaces Investigated by Cyclic Voltammetry and Atomic Force Microscopy. *Electrochim. Acta* **1998**, *43* (9), 1114–1122.
- (29) Chi, Q.; Zhang, J.; Nielsen, J. U.; Friis, E. P.; Chorkendorff, I.; Canters, G. W.; Andersen, J. E. T.; Ulstrup, J. Molecular Monolayers and Interfacial Electron Transfer of Pseudomonas aeruginosa Azurin on Au(111). *J. Am. Chem. Soc.* **2000**, *122* (17), 4047–4055.
- (30) Andolfi, L.; Bruce, D.; Cannistraro, S.; Canters, G. W.; Davis, J. J.; Hill, H. A. O.; Crozier, J.; Verbeet, M. P.; Wrathmell, C. L.; Astier, Y. The electrochemical Characteristics of Blue Copper Protein Monolayers on Gold. *J. Electroanal. Chem.* **2004**, *565* (1), 21–28.
- (31) Rief, M.; Oesterhelt, F.; Heymann, B.; Gaub, H. E. Single Molecule Force Spectroscopy on Polysaccharides by Atomic Force Microscopy. *Science* **1997**, *275* (5304), 1295–1297.
- (32) Giannotti, M. I.; Vancso, G. J. Interrogation of Single Synthetic Polymer Chains and Polysaccharides by AFM-Based Force Spectroscopy. *ChemPhysChem* **2007**, *8* (16), 2290–2307.
- (33) Bustamante, C.; Marko, J. F.; Siggia, E. D.; Smith, S. Entropic Elasticity of Lambda-Phage DNA. *Science* **1994**, *265* (5178), 1599–1600.
- (34) Flory, P. J. *Statistical Mechanics of Chain Molecules*; Interscience: New York, 1969.
- (35) Ainarapu, S. R. K.; Bruijic, J.; Huang, H. H.; Wiita, A. P.; Lu, H.; Li, L.; Walther, K. A.; Carrion-Vazquez, M.; Li, H.; Fernandez, J. M. Contour Length and Refolding Rate of a Small Protein Controlled by Engineered Disulfide Bonds. *Biophys. J.* **2007**, *92* (1), 225–233.
- (36) Walther, K. A.; Gräter, F.; Dougan, L.; Badilla, C. L.; Berne, B. J.; Fernandez, J. M. Signatures of Hydrophobic Collapse in Extended Proteins Captured with Force Spectroscopy. *Proc. Natl. Acad. Sci. U. S. A.* **2007**, *104* (19), 7916–7921.
- (37) Carrion-Vazquez, M.; Oberhauser, A. F.; Fowler, S. B.; Marszalek, P. E.; Broedel, S. E.; Clarke, J.; Fernandez, J. M. Mechanical and Chemical Unfolding of a Single Protein: A Comparison. *Proc. Natl. Acad. Sci. U. S. A.* **1999**, *96* (7), 3694–3699.
- (38) Oberhauser, A. F.; Marszalek, P. E.; Erickson, H. P.; Fernandez, J. M. The Molecular Elasticity of the Extracellular Matrix Protein Tenascin. *Nature* **1998**, *393* (6681), 181.
- (39) Oesterhelt, F.; Rief, M.; Gaub, H. E. Single Molecule Force Spectroscopy by AFM Indicates Helical Structure of Poly(ethylene-glycol) in Water. *New J. Phys.* **1999**, *1* (1), 6.1–6.11.
- (40) Lu, H.; Isralewitz, B.; Krammer, A.; Vogel, V.; Schulten, K. Unfolding of Titin Immunoglobulin Domains by Steered Molecular Dynamics Simulation. *Biophys. J.* **1998**, *75* (2), 662–671.
- (41) Krammer, A.; Lu, H.; Isralewitz, B.; Schulten, K.; Vogel, V. Forced Unfolding of the Fibronectin Type III Module Reveals a Tensile Molecular Recognition Switch. *Proc. Natl. Acad. Sci. U. S. A.* **1999**, *96* (4), 1351–1356.
- (42) Lu, H.; Schulten, K. Steered Molecular Dynamics Simulations of Force-Induced Protein Domain Unfolding. *Proteins: Struct., Funct., Genet.* **1999**, *35* (4), 453–463.
- (43) Lu, H.; Schulten, K. Steered Molecular Dynamics Simulation of Conformational Changes of Immunoglobulin Domain I27 Interpret Atomic Force Microscopy Observations. *Chem. Phys.* **1999**, *247* (1), 141–153.
- (44) Rico, F.; Gonzalez, L.; Casuso, I.; Puig-Vidal, M.; Scheuring, S. High-Speed Force Spectroscopy Unfolds Titin at the Velocity of Molecular Dynamics Simulations. *Science* **2013**, *342* (6159), 741–743.
- (45) Abriata, L.; Vila, A.; Dal Peraro, M. Molecular Dynamics Simulations of Apocupredoxins: Insights Into the Formation and Stabilization of Copper Sites Under Entatic Control. *JBIC, J. Biol. Inorg. Chem.* **2014**, *19* (4–5), 565–575.
- (46) Giroto, S.; Cendron, L.; Bisaglia, M.; Tessari, I.; Mammi, S.; Zanotti, G.; Bubacco, L. DJ-1 Is a Copper Chaperone Acting on SOD1 Activation. *J. Biol. Chem.* **2014**, *289* (15), 10887–10899.
- (47) Fu, Y.; Tsui, H.-C. T.; Bruce, K. E.; Sham, L.-T.; Higgins, K. A.; Lisher, J. P.; Kazmierczak, K. M.; Maroney, M. J.; Dann, C. E.; Winkler, M. E.; Giedroc, D. P. A New Structural Paradigm in Copper Resistance in Streptococcus Pneumoniae. *Nat. Chem. Biol.* **2013**, *9* (3), 177–183.
- (48) Abriata, L. A.; Banci, L.; Bertini, I.; Ciofi-Baffoni, S.; Gkazonis, P.; Spyroulias, G. A.; Vila, A. J.; Wang, S. Mechanism of CuA Assembly. *Nat. Chem. Biol.* **2008**, *4* (10), 599–601.
- (49) Pozdnyakova, I.; Wittung-Stafshede, P. Biological Relevance of Metal Binding Before Protein Folding. *J. Am. Chem. Soc.* **2001**, *123* (41), 10135–10136.
- (50) Wittung-Stafshede, P. Role of Cofactors in Folding of the Blue-Copper Protein Azurin. *Inorg. Chem.* **2004**, *43* (25), 7926–7933.
- (51) Alcaraz, L. A.; Gómez, J.; Ramírez, P.; Calvente, J. J.; Andreu, R.; Donaire, A. Folding and Unfolding in the Blue Copper Protein Rusticyanin: Role of the Oxidation State. *Bioinorg. Chem. Appl.* **2007**, *2007*, 1–9.
- (52) Fuentes, L.; Oyola, J.; Fernández, M.; Quiñones, E. Conformational Changes in Azurin from Pseudomonas Aeruginosa Induced through Chemical and Physical Protocols. *Biophys. J.* **2004**, *87* (3), 1873–1880.
- (53) Huang, Q.; Quinones, E. Assessment of the Stability and Unfolding Pathways of Azurin from Pseudomonas Aeruginosa through the Combination of Denaturing Osmolytes. *Arch. Biochem. Biophys.* **2008**, *477* (1), 175–182.
- (54) Nagy, G.; Wandlowski, T. Double Layer Properties of Au(111)/H₂SO₄ (Cl)/Cu²⁺ from Distance Tunneling Spectroscopy. *Langmuir* **2003**, *19* (24), 10271–10280.
- (55) Friis, E. P.; Andersen, J. E. T.; Madsen, L. L.; Moller, P.; Ulstrup, J. In Situ STM and AFM of the Copper Protein Pseudomonas Aeruginosa Azurin. *J. Electroanal. Chem.* **1997**, *431* (1), 35–38.
- (56) Pompa, P. P.; Bramanti, A.; Maruccio, G.; Cingolani, R.; De Rienzo, F.; Corni, S.; Di Felice, R.; Rinaldi, R. Retention of Native-like Conformation by Proteins Embedded in High External Electric Fields. *J. Chem. Phys.* **2005**, *122* (18), 181102.
- (57) Ron, I.; Sepunaru, L.; Itzhakov, S.; Belenkova, T.; Friedman, N.; Pecht, I.; Sheves, M.; Cahen, D. Proteins as Electronic Materials: Electron Transport through Solid-State Protein Monolayer Junctions. *J. Am. Chem. Soc.* **2010**, *132* (12), 4131–4140.
- (58) Proksch, R.; Schaffer, T. E.; Cleveland, J. P.; Callahan, R. C.; Viani, M. B. Finite Optical Spot Size and Position Corrections in F55

- 656 Thermal Spring Constant Calibration. *Nanotechnology* **2004**, *15* (9),
657 1344–1350.
- 658 (59) Fisher, T. E.; Marszalek, P. E.; Fernandez, J. M. Stretching
659 Single Molecules into Novel Conformations Using the Atomic Force
660 Microscope. *Nat. Struct. Biol.* **2000**, *7* (9), 719–724.
- 661 (60) Rivas-Pardo, J. A.; Alegre-Cebollada, J.; Ramírez-Sarmiento, C.
662 A.; Fernandez, J. M.; Guixé, V. Identifying Sequential Substrate
663 Binding at the Single-Molecule Level by Enzyme Mechanical
664 Stabilization. *ACS Nano* **2015**, *9* (4), 3996–4005.
- 665 (61) Marko, J. F.; Siggia, E. D. Stretching DNA. *Macromolecules*
666 **1995**, *28* (26), 8759–8770.
- 667 (62) Cossins, B. P.; Hosseini, A.; Guallar, V. Exploration of Protein
668 Conformational Change with PELE and Meta-Dynamics. *J. Chem.*
669 *Theory Comput.* **2012**, *8* (3), 959–965.
- 670 (63) Madhavi Sastry, G.; Adzhigirey, M.; Day, T.; Annabhimoju, R.;
671 Sherman, W. Protein and Ligand Preparation: Parameters, Protocols,
672 and Influence on Virtual Screening Enrichments. *J. Comput.-Aided Mol.*
673 *Des.* **2013**, *27* (3), 221–234.
- 674 (64) Jorgensen, W. L.; Maxwell, D. S.; Tirado-Rives, J. Development
675 and Testing of the OPLS All-Atom Force Field on Conformational
676 Energetics and Properties of Organic Liquids. *J. Am. Chem. Soc.* **1996**,
677 *118* (45), 11225–11236.